Optimum high temperature strength of two-dimensional nanocomposites

M. A. Monclús,[1] S. J. Zheng,[2] J. R. Mayeur,[2] I. J. Beyerlein,[2] N. A. Mara,[2] T. Polcar,[3] J. Llorca,[1,4] and J. M. Molina-Aldareguía[1,a]

[1]*IMDEA Materials Institute, C/Eric Kandel 2, 28906 Getafe, Madrid, Spain*
[2]*Los Alamos National Laboratory, Los Alamos, New Mexico 87545, USA*
[3]*Czech Technical University in Prague, Technická 2, Prague 6, Czech Republic*
[4]*Department of Materials Science, Polytechnic University of Madrid, E. T. S. de Ingenieros de Caminos, 28040 Madrid, Spain*

High-temperature nanoindentation was used to reveal nano-layer size effects on the hardness of two-dimensional metallic nanocomposites. We report the existence of a critical layer thickness at which strength achieves optimal thermal stability. Transmission electron microscopy and theoretical bicrystal calculations show that this optimum arises due to a transition from thermally activated glide within the layers to dislocation transmission across the layers. We demonstrate experimentally that the atomic-scale properties of the interfaces profoundly affect this critical transition. The strong implications are that interfaces can be tuned to achieve an optimum in high temperature strength in layered nanocomposite structures. © *2013 Author(s). All article content, except where otherwise noted, is licensed under a Creative Commons Attribution 3.0 Unported License.* [http://dx.doi.org/10.1063/1.4828757]

For increased energy efficiency in many future applications, there is an outstanding need for robust materials that sustain their strength at high temperatures.[1,2] In this regard, nanocomposite metallic multilayers (NMMs) are garnering much interest as promising candidates for materials in extreme conditions. NMMs are 2D nanostructured thin films or sheets that contain alternating layers of dissimilar metals with individual thicknesses far below 100 nm.[3,4] Consequently, NMMs are comprised of an unusually high density of bimetal interfaces. Experiments have shown that these interface-rich composites are several times stronger and structurally more stable after exposure to high-temperature and/or radiation environments than their constituents.[4–9]

The high temperature strength of the NMMs, however, has not been quantified. Current strategies for understanding the influence of temperature on NMM performance typically involve room temperature tests on NMMs that have been previously exposed to elevated temperatures.[6,7,10,11] With the recent progress in the development of the high-temperature nanoindentation (HT-Nano) testing technique,[12–16] it is now possible to study the deformation mechanisms within a localized region of the material at high temperatures, and this capability has been shown very valuable to study two-dimensional nanocomposites.[17,18]

In this work, we combine the HT-Nano technique and crystal plasticity theory to study the effect of interface structure and layer thickness, L, on the high temperature behavior of a model NMM. We discover that a critical layer thickness, L_{crit}, exists at which the reduction in hardness due to temperature is minimal. We propose that L_{crit} corresponds to the layer thickness at which the dislocation mechanism transitions from intralayer slip to interface crossing. The results suggest that the latter mechanism leads to much larger reduction in hardness with temperature. With this critical insight, the possibility of tuning interfaces and their spacing within NMMs to optimize performance at high temperature becomes attainable.

---

[a]Author to whom correspondence should be addressed. Electronic mail: jon.molina@imdea.org

1, 052103-1

Recently, a few experimental and numerical studies have provided clues that the behavior of NMMs is sensitive to the structure of these interfaces,[19–22] which suggests that there is a potential for tuning material properties via interface design. With this in mind, we further explore the influence of interface structure by carrying out HT-Nano testing on two NMMs with different processing histories: physical vapor deposited (PVD) Cu–Nb thin films and accumulative roll bonded (ARB) Cu–Nb sheets. More details on material fabrication can be found in the supplementary material.[23] Extensive experimental work has shown that these two Cu/Nb NMMs have significantly different interface structures. The preferred interface character in the PVD foils is the classical Kurdjumov Sachs (KS) $\{111\}<110>Cu\|\{110\}<111>Nb$ interface, whereas in the ARB NMMs the predominant interface character is $\{112\}<111>Cu\|\{112\}<110>Nb$.[24,25] Both high resolution transmission electron microscopy (HR-TEM) and atomic-scale calculations report that the PVD (KS) interface is atomically flat, while the ARB interface is atomically faceted.[20]

Nanoindentation measurements were performed using a Nanotest Platform 3 Instrument (Micromaterials, Wrexham, UK) fitted with a diamond Berkovich tip. The tests were carried out in inert atmosphere to minimize surface oxidation, and both the sample and indenter tip were heated independently to ensure thermal equilibrium conditions. More details on the HT-Nano testing can be found in the supplementary material.[23] The mean and standard deviations in hardness of the ARB and PVD Cu–Nb NMMs are plotted in Fig. 1, as a function of layer thickness, L, and temperature. For both Cu–Nb NMMs, the room temperature hardness increases or saturates with decreasing L. We find that the strengthening behavior seen in Fig. 1 differs from that of single-phase Cu-based nanomaterials. In nanocrystalline Cu, a reduction in strength (softening) is observed for grain sizes of 10 nm and below.[26] In nanotwinned Cu, strength softening is reported for twin spacings on average 15 nm and below.[27]

The high temperature testing reveals some interesting differences between the PVD and ARB NMMs. First, PVD NMMs are consistently harder than the ARB NMMs at all temperatures. This result is in agreement with the trends observed in recent room temperature studies on Cu–Nb NMMs.[5] Second, the room temperature hardness saturates and the high temperature hardness decreases at $L = 7$ nm for the ARB Cu–Nb NMM. By contrast, the strength continues to increase with decreasing layer thickness for all temperatures in the PVD Cu–Nb NMM, even for the smallest layer thickness of $L = 5$ nm. It has been suggested[4,28] that the plateau or softening signifies the predominance of dislocation glide across interfaces over dislocation glide within individual layers. The mechanism of interface crossing is thermally activated and in principle would be enhanced by elevated temperatures. The results in Fig. 1 are the first indirect experimental evidence that the interfaces in the ARB NMMs are easier for dislocations to cross than those in the PVD NMMs.

It is desirable that nanomaterials strengthen as much as possible with decreasing L, exhibiting a positive and strong size effect (corresponding to the slope of the strength versus layer thickness curve). Interestingly, the size effect in the PVD foils was enhanced by deforming at higher temperatures over the entire layer thickness range (5–30 nm) studied. Similar results were found in ARB NMMs for layer thicknesses above 18 nm. This is the first report of a strength-related size effect that can be enhanced with increasing temperature.

Even more remarkable is the apparent existence of a critical layer thickness L_{crit} at which the reduction in hardness with temperature achieves a minimum. In the case of the ARB NMMs, L_{crit} is around 18 nm. We observe a softening in the ARB material for layer thicknesses below 18 nm. For the PVD material it is apparent that L_{crit} is at most 5 nm. To better elucidate the effect of L on temperature-induced softening, we plot in Fig. 2 the evolution of the ratio between that hardness at 300 °C and the room temperature hardness as a function of L/L_{crit}. When normalized in this way, we observe that the hardness reduction due to temperature decreases as L decreases within $L > L_{crit}$. This trend occurs for both the ARB and PVD NMMs at least in the range for which data are available for both systems, i.e., $1 < L/L_{crit} < 3$). Furthermore, identical trends were observed at 200 °C in PVD NMMs and at 400 °C in ARB NMMs. It bears emphasis that the unprecedented high-temperature effects discussed above would not have been apparent in a post-annealing hardness test, as the room temperature hardnesses of the samples before and after high-temperature testing were similar.

Due to the novelty of the HT results, it is critical to check for compromising effects that can arise during high temperature indentation, like surface oxidation, thermal drift, and/or incorrect
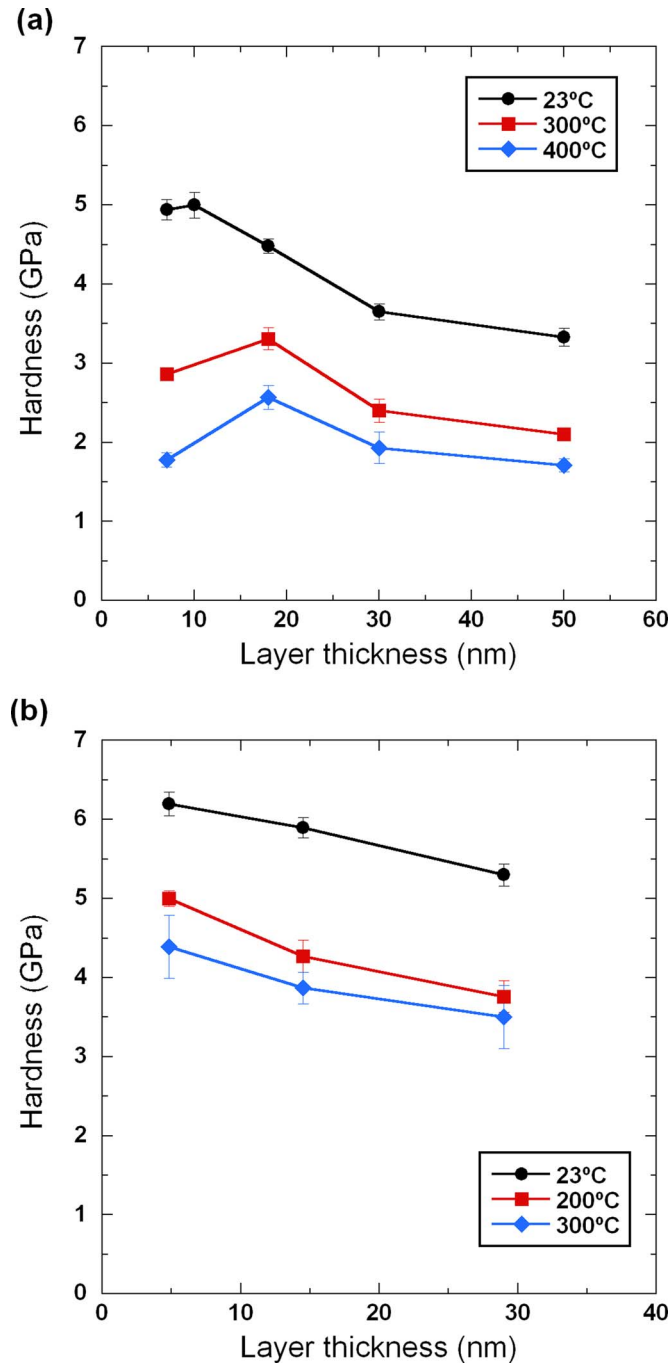
FIG. 1. Indentation hardness vs. layer thickness L for the (a) ARB Cu–Nb NMM at 23 °C, 300 °C, and 400 °C; (b) PVD Cu–Nb NMMs at 23 °C, 200 °C, and 300 °C.

determination of the indenter contact areas due to pile-up effects. Atomic force microscopy scans of room temperature and high temperature indentations (included in the supplementary material[23]) show some degree of pile-up around the indentations, while sink-in behavior was not observed. However, the hardness computed from the measured contact areas using the conventional hardness definition, $H = P/A_c$, was in good agreement with the HT-Nano results shown in the supplementary material,[23] confirming that the high temperature values were free of thermal drift and/or errors in contact area determination due to pile-up effects. Some signs of surface oxidation were visible at
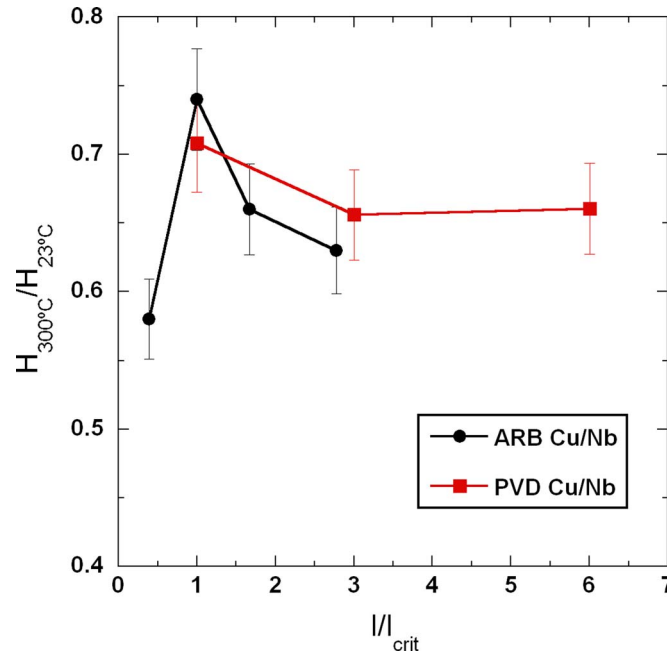
FIG. 2. The 300 °C hardness normalized by the room temperature hardness for each layer thickness as a function of L/L_{crit}, where $L_{crit} \sim 18$ nm for ARB and $L_{crit} \sim 5$ nm for PVD.

300 °C, but not extensively. As a matter of fact, the elastic modulus at 300 °C dropped approximately 10% with respect to the room temperature value (as shown in the HT-Nano results in the supplementary material[23]), independently of L, which is in agreement with the reduction expected for the constituents. Thus, surface oxidation did not affect the hardness results.

   To shed more light on potential deformation mechanisms, such as twinning, shear banding, interfacial sliding, or layer coarsening, selected indents were sectioned by focused ion beam (FIB). Figure 3 shows TEM cross-sectional images of the indents on the PVD Cu/Nb NMMs with $L = 30$ nm for (a) RT and (c) T = 300 °C. Figure 3(e) also shows a cross-sectional image of an indent on the ARB Cu/Nb with $L = 18$ nm at T = 300 °C. The layered structure is well preserved under the indents, irrespective of temperature, with the layer planes rotating to follow the profile of the indentation imprint. No evidence of cracking, shear banding, twinning, or localized deformation was found. No layer coarsening due to temperature annealing was observed, consistent with results from post annealing studies involving no deformation on these materials.[4,6,7]

   To investigate the possibility of interfacial sliding we utilize TEM to measure the differences in the Cu and Nb layer thickness within the deformed region affected by the indent, as shown in the corresponding higher magnification images in Figures 3(b) and 3(d). The average layer thickness after room temperature nanoindentation in the PVD NMM with $L = 30$ nm varied from 29 nm (Cu)/20 nm (Nb) well away from the indent (in agreement with the nominal thickness), to approximately 20 nm (Cu)/15 nm (Nb) at $\sim$250 nm below the indent and finally 18 nm (Cu)/12 nm (Nb) at a few nm under the indent. Likewise, the average layer thicknesses after high temperature nanoindentation varied from 24 nm (Cu)/20 nm (Nb) at $\sim$600–900 nm below the indent (in agreement with the nominal thicknesses), to 20 nm (Cu)/20 nm (Nb) at $\sim$600 nm below the indent and finally, to a final thickness of 16 nm (Cu)/16 nm (Nb) closer to the indent at $\sim$300 nm. Similar trends were observed for the PVD NMM with $L = 5$ nm. These observations suggest that for $L > L_{crit}$, the joined Cu and Nb crystals are co-deforming. Similar measurements in ARB NMMs are more challenging due to the variability of the nominal layer thickness, inherent to this processing method,[5] but the high-resolution electron microscopy (HREM) image of Figure 3(f) shows evidence of confined layer slip within the Cu layers.
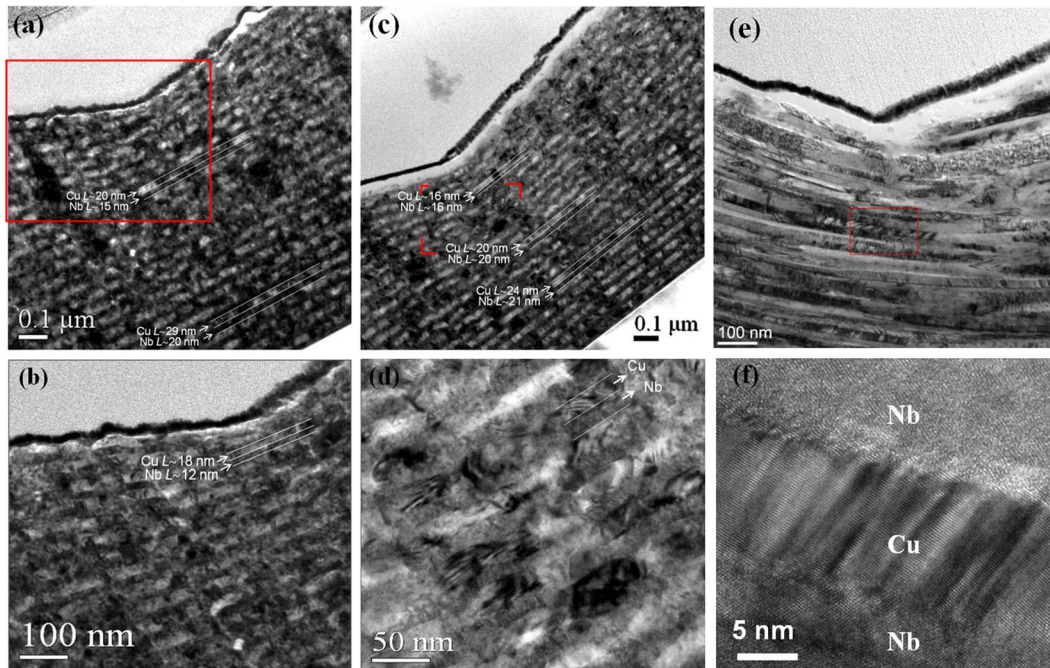
FIG. 3. TEM cross-sectional images of the indents in the PVD Cu–Nb NMM with $L = 30$ nm tested at: [(a) and (b)] RT and [(c) and (d)] T $= 300\,^{\circ}$C. Panels (e) and (f) correspond to the ARB Cu–Nb NMM with $L = 18$ nm tested at $300\,^{\circ}$C. Average layer thicknesses at increasing distances from the indentation tip are included.

To separate the contributions of interface crystallography from other atomic-scale interface properties, we carried out crystal plasticity simulations of a Cu–Nb bicrystal deformed under compression normal to the interface. Temperature and rate effects are incorporated into the anisotropic elasticity and dislocation plasticity laws used to model the Cu and Nb crystals. The model set up considers a Cu single crystal and a Nb single crystal bound together at a common interface. As observed experimentally, the single crystals are constrained to co-deform, by imposing displacement and traction continuity across the interface during deformation. With the above elements, the model can provide basic insight into the combined effect of elastic and plastic anisotropy and temperature. A detailed description of the model is given in the supplementary material.[23] As shown in Fig. 4, the model predicts that the ARB interfaces would result in a lower hardness than the PVD interfaces, in agreement with the experimental observations. The predicted difference of 18% underestimates the actual experimental differences reported here (e.g., PVD NMMs are 30% harder than ARB NMMs for $L = 30$ nm), but agrees with experimental results in other works.[5] The model, however, does not have an explicit dependence on layer thickness as shown in the supplementary material.[23] Therefore, we find that the combined effect of elastic and plastic anisotropy and the predominant texture developed as a function of processing method can account for most of the differences between the hardness of the PVD and ARB processed NMMs with the same layer thickness.

The model also helps in understanding the actual drop of hardness with temperature at different layer thicknesses. Figures 4(a) and 4(b) compare the predicted and measured reduction in hardness (normalized by the room temperature hardness) with temperature for each L and processing method. This normalization was selected in order to isolate the effect of temperature only. As shown, the magnitude of the reduction in hardness as temperature increases from 296 K to 573 K is well captured by the model. In agreement, for $L > L_{\text{crit}}$, the regime where deformation is proposed to be controlled by intralayer slip, the experimental reductions in H are similar for the ARB and PVD materials, being slightly larger for the ARB, a subtle difference that is also predicted (68% reduction for ARB and 66% reduction for PVD). This agreement suggests that, for $L > L_{\text{crit}}$, temperature effects can be
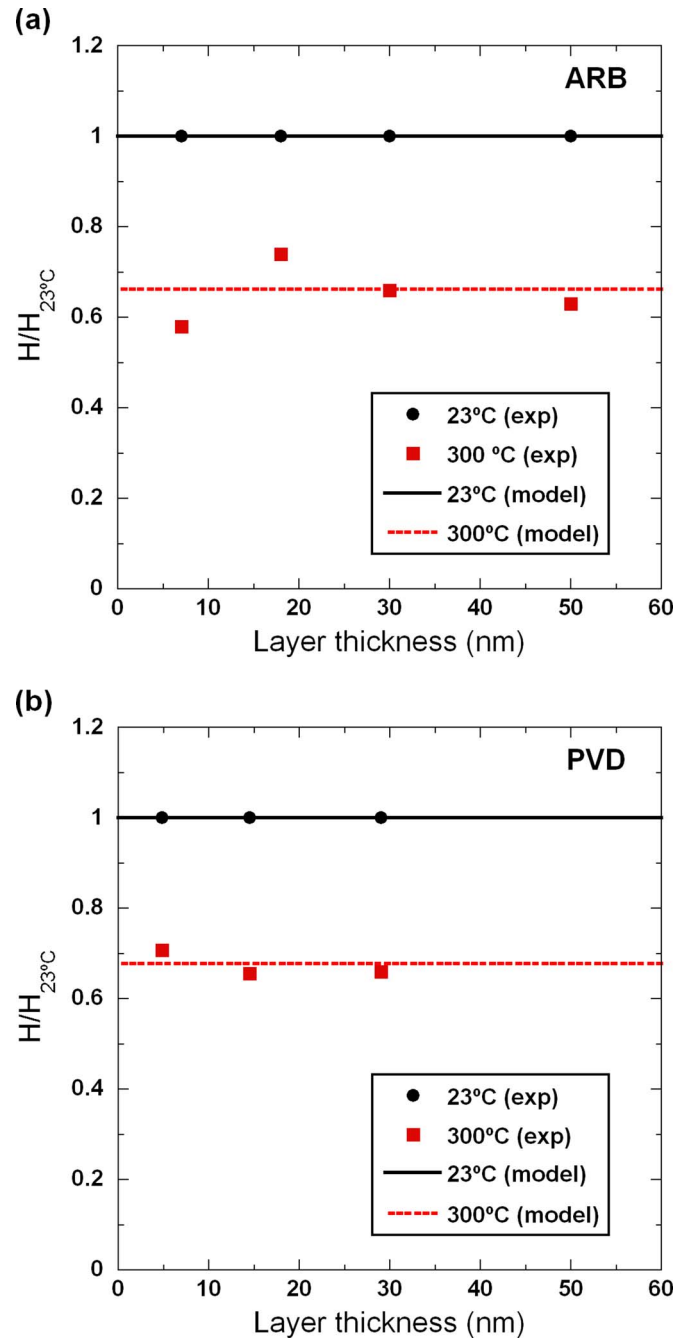
(a)

(b)

FIG. 4. Predicted and measured reduction in hardness (normalized by the room temperature hardness) with temperature for each L for (a) PVD Cu/Nb NMMs and (b) ARB Cu/Nb NMMs.

attributed to higher dislocation mobility at elevated temperatures due to the lower stresses required for thermal activation, which is the thermally activated mechanism assumed in the simulations.

The predictions deviate from the measurements for the ARB NMM with $L = 7$ nm. The calculations assume no change in the thermally activated mechanism with L, and thus, the discrepancy at $L = 7$ nm is consistent with the notion that a change in mechanism occurs at this length scale for the ARB, but not the PVD NMM. Specifically, the ARB and PVD NMM exhibit similar reductions in hardness with temperature above the critical layer thickness L_{crit}, which can be attributed to classical thermally activated dislocation glide. Below L_{crit}, however, another thermally activated

mechanism becomes predominant, likely dislocation-interface crossing, which prevails when the stress to bow out dislocation segments within the nano-layers exceeds the threshold stress for dislocation transmission across the interface.[28,29] Our results on the ARB NMM suggest that the interface crossing mechanism is accompanied by a substantial drop in hardness with temperature. The higher L_{crit} for ARB than PVD can be explained as an interface effect and is in agreement with indirect evidence provided by recent MD calculations suggesting that dislocation transmission across the ARB interface is easier than across the PVD interface.[5,19,20]

In summary, we report on the effect of nanolayer thickness and interface structure on the high-temperature mechanical behavior of two-dimensional nanocomposite metallic multilayers. Our study reveals the existence of a critical layer thickness L_{crit} at which the material is more resistant to softening by elevated temperatures. We show for the first time that L_{crit} depends on interface structure, which provides indirect evidence that L_{crit} corresponds to the layer thickness where the chief deformation mechanism transitions from intralayer slip to interface crossing. These results imply that nano-layer size and interface structure can be tuned to achieve optimal high-temperature strengths in layered nanocomposite structures.

[1] H. Gleiter, Acta Mater. **56**, 5875 (2008).
[2] T. Chookajorn, H. A. Murdoch, and C. A. Schuh, Science **337**, 951 (2012).
[3] J. S. Carpenter, S. C. Vogel, J. LeDonne, D. L. Hammon, I. J. Beyerlein, and N. A. Mara, Acta Mater. **60**, 1576 (2012).
[4] A. Misra, J. P. Hirth, and R. G. Hoagland, Acta Mater. **53**, 4817 (2005).
[5] I. J. Beyerlein, N. A. Mara, J. S. Carpenter, T. R. Nizolek, K. Kang, S. Zheng, J. Wang, T. M. Pollock, J. Mater. Res. **28**, 1799 (2013).
[6] J. S. Carpenter, S. J. Zheng, R. F. Zhang, S. C. Vogel, I. J. Beyerlein, and N. A. Mara, Philos. Mag. **93**, 718 (2013).
[7] S. J. Zheng, I. J. Beyerlein, J. S. Carpenter, K. Kang, J. Wang, W. Z. Han, and N. A. Mara, Nature Commun. **4**, 1696 (2013).
[8] T. Hochbauer, A. Misra, K. Hattar, and R. G. Hoagland, J. Appl. Phys. **98**, 123516 (2005).
[9] K. Hattar, M. J. Demkowicz, A. Misra, I. M. Robertson, and R. G. Hoagland, Scr. Mater. **58**, 541 (2008).
[10] A. Misra, R. G. Hoagland, H. Kung, Philos. Mag. **84**, 1021 (2004).
[11] N. A. Mara, A. V. Sergueeva, T. Tamayo, X. Zhang, A. Misra, and A. K. Mukherjee, Mater. Sci. Eng., A **493**, 274 (2008); Thin Solid Films **515**, 3241 (2007).
[12] J. F. Smith and S. Zheng, Surf. Eng. **16**, 143 (2000).
[13] A. Sawant and S. Tin, Scr. Mater. **58**, 275 (2008).
[14] J. C. Trenkle, C. E. Packard, and C. A. Schuh, Rev. Sci. Instrum. **81**, 073901 (2010).
[15] N. M. Everitt, M. I. Davies, and J. F. Smith, Philos. Mag. **91**, 1221 (2011).
[16] J. M. Wheeler, R. Raghavan, and J. Michler, Mater. Sci. Eng., A **528**, 8750 (2011).
[17] S. Lotfian, J. M. Molina-Aldareguia, K. E. Yazzie, J. Llorca, and N. Chawla, Philos. Mag. Lett. **92**, 362 (2012); J. Electron. Mater. **42**, 1085 (2013).
[18] S. Lotfian, M. Rodríguez, K. E. Yazzie, N. Chawla, J. Llorca, J. M. Molina-Aldareguía, Acta Mater. **61**, 4439 (2013).
[19] R. F. Zhang, T. C. Germann, X. Y. Liu, J. Wang, and I. J. Beyerlein, Scr. Mater. **68**, 114 (2013).
[20] I. J. Beyerlein, J. Wang, and R. F. Zhang, Acta Mater. **61**, 7488 (2013).
[21] I. J. Beyerlein, J. Wang, K. Kang, S. J. Zheng, and N. A. Mara, Mater. Res. Lett. **1**, 89 (2013).
[22] I. J. Beyerlein, J. Wang, and R. F. Zhang, APL Mat. **1**, 032112 (2013).
[23] See supplementary material at http://dx.doi.org/10.1063/1.4828757 for details on materials fabrication; details on high temperature nano-indentation; data supporting Figs. 1 and 2; and crystal plasticity model description.
[24] J. S. Carpenter, R. J. McCabe, I. J. Beyerlein, T. A. Wynn, and N. A. Mara, J. Appl. Phys. **113**, 094304 (2013).
[25] S.-B. Lee, J. E. LeDonne, S. C. V. Lim, I. J. Beyerlein, and A. D. Rollett, Acta Mater. **60**, 1747 (2012).
[26] J. Schiotz and K. W. Jacobsen, Science **301**, 1357 (2003).
[27] L. Lu, X. Chen, X. Huang, and K. Lu, Science **323**, 607–610 (2009).
[28] S. L. Lehoczky, Phys. Rev. Lett. **41**, 1814 (1978).
[29] J. D. Embury and J. P. Hirth, Acta Metall. Mater. **42**, 2051 (1994).